Late Oligocene midlatitude warming and temperate Early Miocene from alkenone-derived Sea Surface Temperature estimates

José Guitián[1] and Heather M Stoll[1]

[1]Geological Institute, ETH Zürich, Switzerland
Corresponding author: José Guitián (jose.guitian@erdw.ethz.ch)

Key Points:

- Alkenone-derived sea surface temperatures show cold conditions related with the MOGI, and confirms the long term warming during the Late Oligocene.
- This record highlights the different amplitudes of Late Oligocene warming obtained from different proxies and locations.

Abstract

Large Antarctic ice volume changes characterized the middle to Late Oligocene and the first million years of climate evolution during the Miocene. However, the sea surface temperature (SST) evolution over this period remains poorly constrained, as only a few records from contrasting proxies are available. In this study, we present a long-term alkenone-derived SST record from sediments drilled by the Ocean Drilling Program (ODP) at Site 1168 in the west Tasmanian Sea spanning 29.8 Ma to 16.7 Ma. The SST record reaffirms that the long term warming in the Late Oligocene linked to the end of the Middle Oligocene Glacial Interval can be recognized also at mid-to-high latitudes of the Southern Hemisphere. Stable average temperatures are present from 24.5 to 22 Ma, and then decrease 2°C into the Miocene until they stabilize by 20.1 Ma. The reconstructed temperatures are highly variable in the warm Late Oligocene waters, and more stable and slightly colder in the Early to Middle Miocene. We confirm that this temperature trend is not an artefact of the latitudinal drift of the site, as the temperature anomaly relative to the modern water temperature at the paleolocation confirms the SST trends of the Oligocene. This is the first alkenone-derived record to show the cold conditions related with the Middle Oligocene Glacial Interval in the Southern Ocean and gradual warming in the latest Oligocene.

1. Introduction

Suborbital resolution deep-sea benthic oxygen isotope records reveal large oscillations, at both orbital and multimillion-year timescales, over the Oligocene to Early Miocene time interval (De Vleeschouwer et al., 2017; Westerhold et al., 2020; Zachos et al., 2001) which are interpreted to reflect large variations in the Antarctic ice volume and temperature oscillations at the deep-water formation regions (Liebrand et al., 2017; Pekar and DeConto, 2006). The Oligocene presents a 2.5 myr long period of enriched $\delta^{18}O$ described as the Middle Oligocene Glacial (MOGI) (Liebrand et al., 2017), followed by a long term shift towards lighter values from 26.5 Ma attributed to a Late Oligocene Warming (LOW) (Pekar et al., 2006; Villa and Persico, 2006). However, this deep-sea interpretation of climate has not yet been widely contrasted with long term and high-resolution sea surface temperature (SST) records from high latitude regions.

The majority of available SST records spanning the Oligocene and Miocene are based on organic biomarkers, glycerol dialkyl glycerol tetraethers (GDGTs) TEX_{86} index and these present some paradoxes. GDGT-based estimates suggest similar absolute temperature at two tropical sites (O'Brien et al., 2020; Zhang et al., 2013) as at mid-to high latitude sites in the North and South Atlantic Ocean (O'Brien et al., 2020; Super et al., 2018), an absence of temperature gradients difficult to reconcile with climate models. While some of these records suggest long-term SST trends superimposed on higher frequency variability, GDGTs-derived temperatures from the Southern Ocean high latitude Site 1356 do not resolve multimillion year trends such as the MOGI or the Late Oligocene warming (Hartman et al., 2018) but do suggest high amplitude SST changes over orbital timescales starting at the Early Oligocene.

The few long-term SST records for the Oligocene to Early Miocene estimated from the long−chain alkenone unsaturation ratio ($U^{k'}_{37}$) are restricted to mid latitude sites in the North Atlantic, where they define punctuated excursions and multimillion-year variations coincident with the benthic isotope records (Guitián et al., 2019; Liu et al., 2018). However, these records are interrupted during part of the MOGI, potentially underestimating the amplitude of its temperature change, and during the Early Miocene.

Additional SST reconstructions are required to explore the temperature variability at mid-to-high latitudes sites, especially in the Southern Ocean to contrast with global benthic $\delta^{18}O$ temperatures at deepwater formation regions and with sea level reconstructions. This together with interpretations of past oceanographic patterns would improve the knowledge of the climate state over the Oligocene.

In this study, we present a new alkenone-based SST record from $U_{37}^{k'}$index over the Middle Oligocene to Early Miocene sediments recovered from the West South Tasmanian Rise by the Ocean Drilling Program (ODP) at Site 1168 which had a estimated paleolatitude of 54°S by the middle Oligocene (Exon et al., 2001), ideal for providing a high latitude Southern Hemisphere view on surface ocean temperature. In this period, ODP 1168 transitions from carbonate-poor claystone to clay-bearing carbonate rich sediments relatd to deepening of the basin. Application of recent analytical techniques allow better separation of both C_{37} and C_{38} long chain alkenones to identify alkenone indices that verify $U_{37}^{k'}$-calculated SST trend despite the change in coastal proximity of the site. The site location on the Tasmanian Rise was influenced by the gradual northward movement of the Australian plate, which widened the gateway between Australia and Antarctica and strengthened the exchange of water masses between the south Pacific and the Indian Ocean (Exon et al., 2002; Pfuhl and McCave, 2005; Pfuhl et al., 2004; Scher et al., 2015; Stickley et al., 2004b). We account for this latitudinal movement in the examination of temperature trends and gradients. Our SST record has an average 350 ky resolution, and although it exihibits high frequency variation potentially related to orbital cycles, coherent significant multi-million year scale trends in mean SST are evident. We compare our records with the existing SST reconstructions in the Southern Ocean to explore the evolution of temperature gradients, and also contrast with available globally distributed estimates to identify the magnitude of the defined long-term trends at both hemispheres. Furthermore, our record is compared with the global benthic oxygen isotopes, sea level reconstructions as well as with bottom water temperatures measures.

This record therefore extends previous reconstructions of the Late Oligocene and Early Miocene temperature evolution in mid-to-high latitudes in the Southern Ocean and around Antarctica, and improves the knowledge of climate states in a time interval where most existing CO_2 estimates show controversial evolution.

2. Setting and sediments

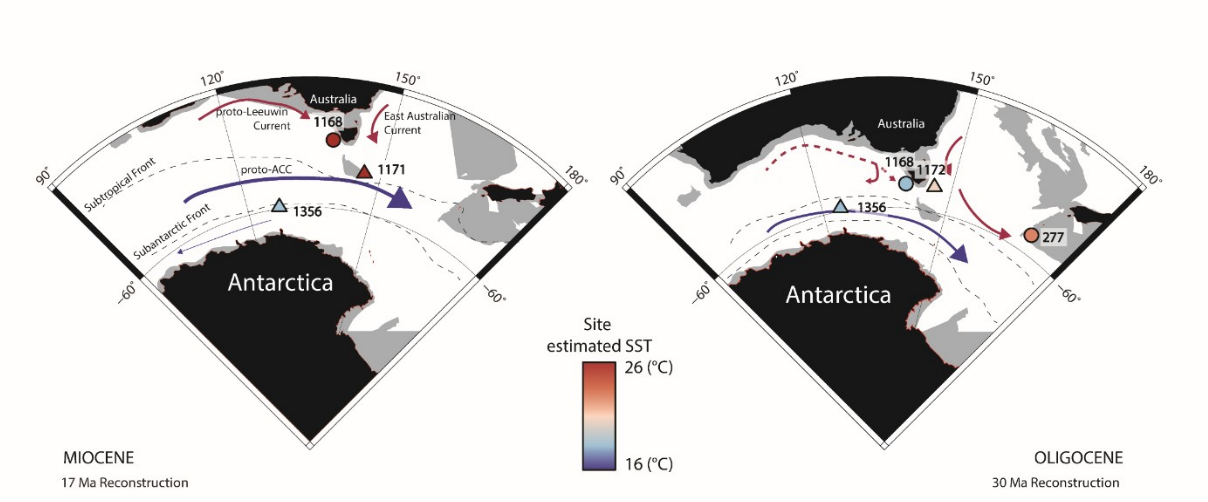

Figure 1. Reconstructed map of the study area with inferred surface ocean currents (red and blue solid and dashed lines) and convergent fronts (black dashed lines) (Salabarnada et al., 2018; Scher et al., 2015). Black fill denotes the paleo-location of the currently exposed continental area while the grey shading shows the continental rise. Site locations are shown with triangles and circles for GDGT-derived and alkenone-derived SST respectively, and are coloured as a function of the estimated paleotemperature at each timeslice after published SST estimates (Hartman et al., 2018; Houben et al., 2019; Leutert et al., 2020; Liu et al., 2009) (Table S1).

Site ODP 1168 is located in the offshore of the Australian plate at the western margin of Tasmania (Figure 1), at 43° 36.57'S and 139 144° 24.76'E, and 2463m water depth, drilled within a graben-developed basin with sediment accumulation since the latest Eocene (Exon et al., 2001). It is one of the few locations in high paleolatitudes with relatively carbonate rich sequences for this time interval (Exon et al., 2001).

During the Late Eocene the area was within a system of migrating deltas and relatively restricted basins (Exon et al., 2001) which then led to a progressive deepening to 2.5 km by the end of the Miocene (Exon et al., 2001; Hill and Exon, 2004; Stickley et al., 2004b) as a consequence of the northward shift of the Australian continent. For the interval in our study, a recent synthesis of data including seismic stratigraphy suggest deepening from a paleodepth of about 700 m at 29 Ma to a depth of 1500 m for Site 1168 area by 21 Ma (Hochmuth et al., 2020). The deltaic coastline systems along the western Tasmanian continental margin and nearby isolated islands were most likely the source of material deposited at Site 1168 over the Early Oligocene (Exon et al., 2001; Hochmuth et al., 2020). Although carbonate content and preservation of biogenic calcite start to already increase along the Early Oligocene, C/N ratios suggest that terrestrial organic matter input was predominant before 30.5 Ma (Exon et al., 2001). The lines of evidence suggest that, the gradual subsidence and increasing distance from the coast driven by the tectonic context in the area (Hill and Exon, 2004), resulted in a progressive change from dominance of shallow terrigenous sediments to pelagic carbonates during the Middle Oligocene (Exon et al., 2001). Therefore, the continuous stratigraphic sequence at Site ODP 1168 evolves from shallow-marine silty claystone in the latest Eocene and Early Oligocene, transitioning to clay-rich chalk and nannofossil ooze in the Miocene (Exon et al., 2001).

The paleoceanographic context is also paced by the progressive deepening of the Tasmanian Gateway, which played an important role in paleocirculation changes. The initial exchange of marine waters through the Gateway started during the Eocene (Stickley et al., 2004b). By 30 to 29 Ma, neodymium isotopes from fish teeth (recording bottomwater chemistry) at Site 1168 and the nearby but deeper Site 1172 had descended from typical Pacific signatures to values identical to the the Indian and Atlantic endmember, indicative of eastward flowing deep current from the Indian into the Pacific through an open gateway, inferred to indicate the onset of the ACC (Scher et al., 2015).

For this study, 81 samples have been selected from Site 1168 Hole A in the 720 to 274 mbsf section of the recovered sequence. During our interval of focus, sediments are characterized by a gradual increase in %$CaCO_3$ content, from 10 % up to 70 %; particle size is dominantly silt and clay with sand content below 20 %, and Total Organic Carbon (TOC%) below 2% (Exon et al., 2001). This contrasts with older deposits, which feature higher TOC, larger grain size and lower carbonate content typical of nearshore conditions.

Today, Site 1168 is located north of the Polar Front (PF), Subtropical Front (STF) and the northern boundary of the Antarctic Circumpolar Current (ACC). Nevertheless, the site location has drifted in latitude following the Australian plate spread to the north away from Antarctic continent. Paleogeographic models estimate 7 degrees northward shift from 30 Ma to 15 Ma (Torsvik et al., 2012) from a paleolatitude of 54.8°S to a latitude of around 48.9°S. In addition, frontal position has also evolved since the Oligocene. The reconstructed paleoposition of the PF based on microfossil assemblages of diverse cores in the area is in the range from 60°S to 66°S (Scher et al., 2015). Although several reference frames of latitude drift have been reconstructed (O'Neill et al., 2005; Torsvik et al., 2008; Torsvik et al., 2012), in all of them Site 1168 appear to transit northward of the PF around 30 Ma and in no case later than 29.5 Ma.

The age model for Site 1168 has been in continuous revision since the first published shipboard reference based on biostratigraphy and magnetostratigraphic reversals (Pfuhl and McCave, 2003; Stickley et al., 2004a). Subsequent further refinements in nanofossil biostratigraphy provide a new detailed age model across the Oligocene to Miocene transition (Mcgonigal, 2004) which agrees well with previous chronology. In this study, we apply chronology updated to the Geological Time Scale from Gradstein et al. (2012) by Guitián et al. (2020) and modelled based on the original magnetostratigrahy and biostratigraphy (Stickley et al., 2004a). Although original magenstostratigraphy from 22 Ma to 21 Ma have uncertainties related to the weak magnetic signal, and there is some disagreement with biostratigraphic points (Mcgonigal, 2004; Stickley et al., 2004a) we consider this chronology sufficiently resolved for the long term and low-resolution scale of this study.

3. Methods

3.1 Organic extraction and biomarker analysis.

Preparation of organic samples was performed on a total lipid extract (TLE). For the selected samples, TLE was obtained from approximately 30g of freeze-dried disaggregated sediment extracted with an Accelerated Solvent Extractor 350. Solvent CH_2Cl_2/MeOH (9:1 v/v) in for four static cycles was used at 100°C. Once concentrated under N2 purified stream, TLE was saponified with ~2 ml of a 0.5 M KOH in 95:5 MeOH:H_2O (optima grade). The neutral fraction was obtained using 0.5ml of Hexane shaking and pipetting out the saponified fraction three times. Silica gel column chromatography was then applied for further purification by eluting 4ml of Hexane, 4ml of CH_2Cl_2 and 4ml of MeOH for separation of the neutral fraction into a hydrocarbon fraction, a ketone fraction, including the long chain alkenones (LCA) and a polar fraction respectively.

Additional sample resolution was obtained from samples extracted at Utrecht University by Milestone Ethos X microwave system. CH_2Cl_2:MeOH 1:1 v/v was added to powdered and freeze-dried sample. This set of samples was not saponified, but only purified by column chromatography straight after the extraction splitting the TLE into an apolar, ketone and polar fraction using Hexane: CH_2Cl_2 (9:1 v/v), Hexane: CH_2Cl_2 (1:1 v/v) and CH_2Cl_2:MeOH (1:1 v/v).

Quantification of alkenones was performed by a Thermo Scientific Trace 1310 Gas Chromatograph (GC) equipped with a Flame Ionization Detector (FID) at ETH Zurich. The GC column was an Agilent VF – 200ms (60 m X 0.25 mm X 0.25 mm) coupled to a 5-m guard column from where 4 to 5 cm were trimmed before every sequence to avoid condensation or stack of non-eluting compounds. Helium at 2-ml/min was used as carrier gas flow. The GC oven was set at 60°C for one minute after injection and then ramped at 20°C/min to 255°C, 3°C/min to 300°C and finally 10°C/min to 320°C to be held 5 min. Several replicates and injection of an in-house alkenone standard (provided by G. O'Neil (Western Washington University) and C. M. Reddy (Woods Hole Oceanographic Institution) as well as n-alkane standards at every sequence were used to monitor the precision of the measurement and the performance of the instrument yielded a precision of 0.012 $U_{37}^{k'}$units.

3.2 Alkenone unsaturation indices and Sea Surface Temperature estimations

We used the distribution and abundance of present long chain alkenones (LCA) biosynthesised by the haptophyte marine algae coccolithophores, to estimate previously defined carbon unsaturation indices. For temperature estimations, we applied the commonly used in palaeoceanography $U_{37}^{k'}$ratio (Brassell et al., 1986; Prahl and Wakeham, 1987), based on the relative abundances of two compounds, $C_{37:2}$ and $C_{37:3}$, each with 37 carbon atoms and two or three carbon double bonds respectively:

$$U_{37}^{k'} = \frac{C_{37.2}Me}{(C_{37.2}Me + C_{37.3}Me)}$$

The 37-carbon methyl ketones, possess more double bonds with colder water temperatures. Alkenone-derived SST record was estimated based on the $U_{37}^{k'}$ unsaturation index using the BAYSPLINE calibration from Tierney and Tingley (2018). Although for high $U_{37}^{k'}$in the BAYSPLINE calibration, uncertainties become larger, this calculation has the advantage of propagating the error through the SST calculations since errors are not uniform across the entire temperature range.

The $U_{37}^{k'}$temperature calibrated with recent sediment samples and tested with culture studies for modern LCAs strains is widely assumed to yield accurate temperatures for earlier times in the Cenozoic. However, it has been proposed that non-thermal factors such as haptophyte algae assemblage composition or surface ocean productivity could affect the long chain alkenone distribution and abundances and therefore could bias the initial alkenone-derived SST reconstruction (Conte et al., 1998; Prahl et al., 2006) since $U_{37}^{k'}$ is calibrated to specific environment strains. Particularly for marginal ocean environments, it is proposed that environments with strongly contrasting salinity may host different alkenone-producing strains (Kaiser et al., 2017; Longo et al., 2016).

The analytical instrumentation applied in this study (mid-polarity stationary phase column, VF-200ms) identifies both C_{37} and C_{38} methyl and ethyl long chain alkenones with good resolution in the chromatogram (Longo et al., 2013). Therefore, when the C_{38} had sufficient concentration in our samples and were well resolved, we report $U_{38Me}^{k'}$ (Conte and Eglinton, 1993) derived from the distribution of the C_{38} methyl substitution:

$$U_{38Me}^{k'} = \frac{C_{38.2}\,Me}{(C_{38.2}\,Me + C_{38.3}\,Me)}$$

The index$U_{38Me}^{k'}$ has been previously suggested to be a more robust indicator of temperatures in settings which may be inhabited by diverse communities of haptophytes including members of Group II and Group I phylogenies as well as the typical marine Group III alkenone producers following the phylogenetic naming convention of Theroux et al. (2010). Today such mixtures of communities are most common in coastal or estuarine environments. These communities appear to have diverse intercepts between $U_{37}^{k'}$ and temperature (D'Andrea et al., 2016), potentially confounding paleotemperature estimates if the community composition is varying or is not represented by the same community as the calibration equation. In such settings the index$U_{38Me}^{k'}$ is expected to be more reliable because while C_{37} alkenones may be produced by Group I, II, and III, the relative production of methyl C_{38} is much greater in Group III marine alkenone producers, making its source and calibration therefore more restricted (Zheng et al., 2019).

To additionally evaluate the potential paleoceanographic conditions that might have influenced the SST reconstruction, we computed further indices between C_{37} and C_{38} alkenones. The ratio between them C_{37}/C_{38} (Rosell-Melé et al., 1994); relationship between all C_{37} and the ethyl C_{38} alkenones $C_{37}/C_{38}Et$; the ratio between the methyl and ethyl C_{38} alkenones $C_{38}Me/C_{38}Et$, and the specific compound RK2 ratio between di-unsaturated C_{37} methyl and C_{38} ethyl alkenones ($RK2=C_{37.2}Me/C_{38.2}Et$) (Zheng et al., 2019).

4. Results

4.1 Long Chain Alkenones abundance and distribution

The total of 53 samples extracted at ETH Zurich had diverse distribution of organic compound in the ketone fraction examined (Figure 2). The subset of samples which were not saponified but only purified with column chromatography present, as expected, a greater diversity of organic compounds, however the samples younger than 25 Ma, and some prior to 25 Ma, had well resolved and quantifiable LCA (Figure S1).

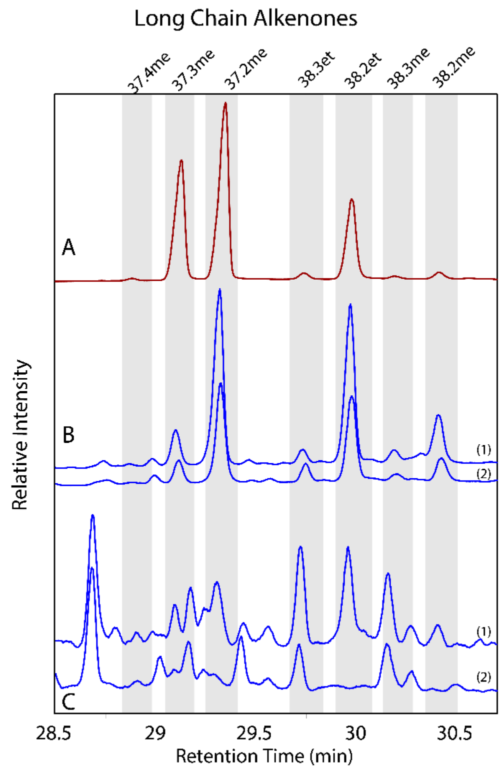

Figure 2. Illustrative chromatograms and long chain alkenones peaks of Site 1168 samples. (**a**) In-house alkenone standard. (**b**) Examples of well-resolved alkenones samples (1= 1168A-41X-4 W, 57.0-61.0 cm 22.1 Ma; 2= 1168A-37X-4 W, 52.0-58.0 cm 20.4 Ma). (**c**) Sample examples of unresolved chromatogram with unknown compounds (1= 1168A-61X-1 W, 45.0-51.0 cm 27.9 Ma; 2= 1168A-75X-4 W, 130.0-136.0 cm 31 Ma.

Most of the samples older than 25.5 Ma had unresolved compounds in the chromatogram in the retention time range corresponding to LCAs (Figure 3). These coeluting compounds complicate and in many cases preclude identification and quantification of chromatogram peak area. Only 8 samples in this segment featured chromatograms clean enough to quantify the various alkenones with confidence, including 3 where saponification was not performed.

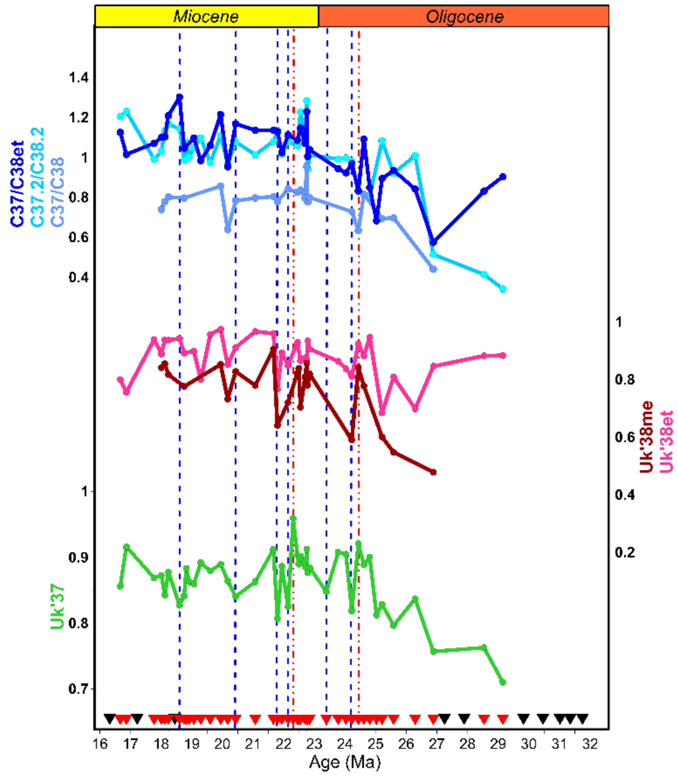

Figure 3. Biomarker results from ODP Site 1168. Vertical dashed lines after 25.5 Ma highlight lower and higher $U^{k'}_{37}$ than the mean variation with blue and red colours respectively. Bottom black and red triangles show samples with respectively unresolved and well resolved $C_{37.3}$ and $C_{37.2}$ compounds.

In contrast, the interval younger than 27 Ma is characterized by well resolved and identified long chain alkenones. In the ketone fraction, most of the C_{37} and C_{38} LCAs feature peaks with good shape and no coelution. From the chromatograms of this set of clean samples we are able to identify always two of the C_{37} ketones, the less abundant tri- and more abundant di-unsaturated alkenones. The C_{38} ketones, when all are present and resolved, have similar concentrations as the C_{37} being the $C_{38.2}$ ethyl ketone the most abundant. Some samples additionally presented C_{39} ethyl alkenones, however always under the detection limit for the isotopic analysis attempted in this study.

The ratio between all C_{37} and C_{38} alkenones gradually increases from 0.4 at 26.8 Ma to 0.9-1 by the Miocene (Figure 3). The compound specific ratio $C_{37.2}/C_{38.2}$ also gradually increases from 0.3 in the first identified sample at 29.2 Ma to 1.2 by the end of the record in the Miocene. The C_{37}/C_{38}Et ratio follows a similar trend and values as the total C_{37}/C_{38} and $C_{37.2}/C_{38.2}$, with the exception of the two oldest samples, which feature high ratios of C_{37}/C_{38}Et.

For the studied time interval, $U^{k'}_{37}$ratio is presented and discussed for 43 samples from the most purified set, while the C_{38} unsaturation index $U^{k'}_{38Me}$is resolved only in 24 samples. The oldest samples measured, at 29.2 Ma, feature the lowest $U^{k'}_{37}$of 0.7. Subsequently $U^{k'}_{37}$rises to 0.95 at 22.3 Ma, before stabilizing around 0.88 in the Early Miocene. The Index $U^{k'}_{38Me}$ follows a similar pattern despite the lower resolution. The highest correlation with $U^{k'}_{37}$is found in the $U^{k'}_{38Me}$index (r2=0.82) followed by the specific compound ratio $C_{37.2}/C_{38.2}Et$ (r2=0.6) (Figure 4).

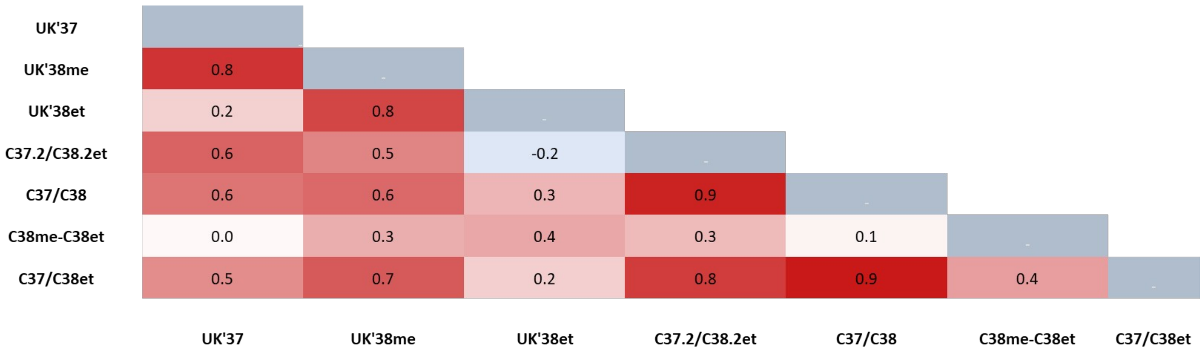

Figure 4. Correlation plots between ODP 1168 reported alkenone indices.

Because of the large sample volume required for LCA analysis, we have processed sediment samples in a way that permits intact foraminifera to be extracted following solvent extraction rather than aggressively grinding sediments. Because the ease of disaggregation differs among samples and may affect alkenone yields, we have not sought to rigorously quantify the alkenone concentration per grams sediment nor applied internal standards to develop such quantification. Rather, we can broadly estimate the abundance from comparison of individual organic compound peak areas compared with those of consistency standards of n-alkane C_{39} and C_{40} standards in the same analytical run. This approach does reveal if there are large changes in alkenone concentration. In the saponified samples with clear chromatograms, the concentrations of long chain alkenones C_{37} as well as C_{38} ranged between 10 and 200 ng per grams of dry sediment. A single sample at 19.9 Ma features more than 1000 ng per gram. No relationship is found between obtained temperature related indices, $U^{k'}_{37}$and $U^{k'}_{38Me}$, and the estimated concentration of alkenone C_{37} and C_{38} (Figure S1).

Few sample chromatograms present a resolved organic compound at the same retention time of tretraunsaturated $C_{37.4}$ alkenone of our in-house alkenone standard. The potential percentage of $C_{37.4}$ over the total C_{37} is presented at Supplement Figure 1; the highest estimated concentrations are around 2.6%. Samples containing this compound coincide with three lower than average $U^{k'}_{37}$values. Given the complex compound distribution in Site ODP 1168, and the intermittent presence of this peak, we propose that further GC-MS evaluation is required prior to any interpretations.

4.2 Late Oligocene to Early Miocene SST estimations

BAYSPLINE-derived SST using the $U^{k'}_{37}$index range from 19°C to 29°C in the Late Oligocene to Early Miocene at ODP Site 1168 (Figure 5). Data show long-term warming in the Late Oligocene of 5°C, from 29 Ma to 24.7 Ma coincident with the Late Oligocene Warming originally identified in benthic isotope records (Pekar et al., 2006; Villa and Persico, 2006). Average temperatures are stable around 25°C through the Oligocene to Miocene transition to later cool down 2°C into the Miocene from 22.6 to 21.1 Ma. Later on stable temperatures around 24.5°C characterize the record. Within the long-term trend, higher frequency variation is of larger amplitude through the Late Oligocene Warming, the Oligocene Miocene transition and through the first Myr. of the Miocene. Posterior data across rest of the studied Miocene is within a 2°C amplitude.

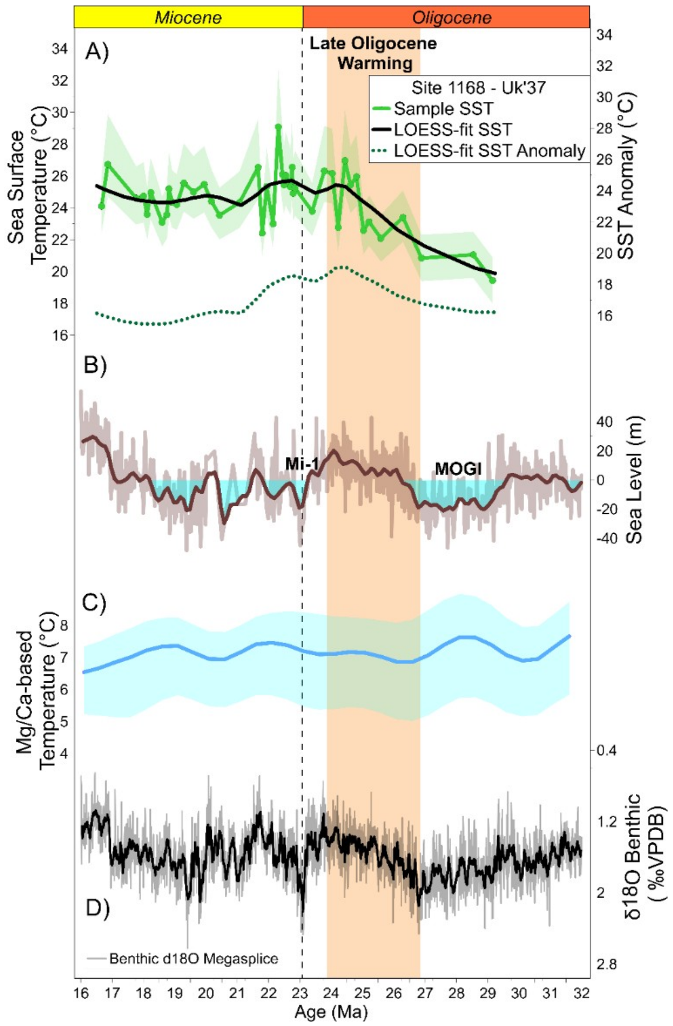

Figure 5. SST reconstruction for ODP Site 1168 and global climatic signatures. (**a**) Mean SST Bayspline reconstruction with 1-sigma CI (green). Black line describe fitted data with LOESS model. Dashed line shows SST anomaly reconstruction. (**b**) Sea level reconstructions from Miller et al. (2020). Filled blue colour are intervals with negative sea level. (**c**) Bottom water Mg/Ca-based temperature estimates with 2-sigma uncertainty reconstructed by Cramer et al. (2011). (**d**) Benthic Megasplice $\delta^{18}O$ from De Vleeschouwer et al. (2017). Vertical orange band shows the interval identified as the Late Oligocene Warming.

5. Discussion

5.1 Confirmation of marine-dominated SST signal with LCA

Changes in the nature of sedimentation at Site 1168 settings is reflected in the diversity of organic compounds in the analysed samples. The oldest samples present in the ketone fraction a complex distribution of compounds (i.e. Figure 2), especially before 29 Ma. Those observations, together with the high TOC % (>1%wt) and low $CaCO_3$ (<10%) are with the marginal and deltaic marine settings in the Early Oligocene at the location (Exon et al. (2001);

Figure S1). Only after the decline in TOC% to below 0.8%, the resolution and identification of LCAs is better. The preservation of organic compounds might be affected by changes in diagenetic reactions as the site gradually subsides into deeper, more oxygenated waters, potentially moving out of the oxygen minimum zone by 29 Ma (Exon et al., 2001; Hill and Exon, 2004; Hochmuth et al., 2020). The later simultaneous gradual opening of the restricted basin might lead to an increase in ventilation and oxygenation of the regional water column following the invigoration of currents through the opening gateway. Oxygen exposure time determines the overall loss of alkenones. Although some have proposed that more unsaturated compounds are easier to degrade (Brassell, 1993; Rechka and Maxwell, 1988), other results show less conclusive selectivity of degradation (i.e. Gong and Hollander, 1999; Grimalt et al., 2000) and affirm there is no consistent evidence of selective degradation of diunstaurated versus tri-unsaturated alkenones at depleted oxygen waters or sediments. This syntheses propose that alkenone degradation does not affect the ratio between C_{37} alkenones in sediments nor while settling in the water column (Grimalt et al., 2000).

Despite the observed change in environment conditions, our alkenone based proxy $U_{37}^{k'}$show a trend that is in agreement with the observed $U_{38Me}^{k'}$index (Figure 3).

The main coccolithophore skeleton preserved at Site 1168 sediments are the reticulofenestrids group (Guitián et al., 2020; Wei et al., 2003). They are known to be the ancestors of the modern open ocean alkenone producers, *E. huxleyi* and *G. oceanica*, (Marlowe et al., 1990; Volkman et al., 1980; Young, 1998) included in Group III (Theroux et al., 2010). Modern estuarine environments and saline lakes are dominated by *I. galbana*, *R. lamellosa* from Group II which do not leave mineralized fossils in sediments, and they may have different $U_{37}^{k'}$ to temperature calibrations than Group III (D'Andrea et al., 2016). Today, some marine environments allow the coincidence of both open ocean alkenone producers and the Group II alkenone producers (Longo et al., 2013; Zheng et al., 2019).

Since algae from brackish to saline environments generally do not generate as C_{38} methyl alkenones as the ocean water ones (Lopez et al., 2005; Zheng et al., 2019; Zheng et al., 2017), Zheng et al. (2019) suggested that temperature reconstructions from the ratio $U_{38Me}^{k'}$will provide robust estimations which are free from artefacts of changing relative abundance of Group II and Group III haptophytes algae. We present unsaturation indices from the C_{38} LCAs (Figure 3; Figure S1), however, $U_{38Me}^{k'}$could be calculated for only 24 samples, when large changes in $U_{37}^{k'}$are found, (ie from 29 to 24 Ma),$U_{38Me}^{k'}$covary with $U_{37}^{k'}$, (r2=0.82).

One more evidence of the marine origin of the $U_{37}^{k'}$involved lipids is the covariance obtained from the $C_{37.2}$Me and $C_{38.2}$Et relationship, RK2 index (Zheng et al., 2019) (Figure 3). Both LCAs are produced among different species groups but their ratio is more sensitive to temperature in the open marine environments strains (Zheng et al., 2019). In our dataset, the RK2 is positively correlated with the temperature related indices, which suggests the open water source of LCAs (r2: 0.64$U_{37}^{k'}$; r2=0.51 $U_{38Me}^{k'}$) (Figure 4). This evidences lead to interpret the long-term trend in $U_{37}^{k'}$as most likely derived from ocean water algae assemblage and the temperature estimates are not biased due to influence of other alkenone producing families such as those found in modern coastal or low saline environments.

Once marine alkenone source is defined, the shallow position of ODP Site 1168 sedimentation likely support little horizontal drift of the organic compounds as settling down from the surface. As the surface paleo circulation followed the west-east direction with the Proto – Leeuwin current, parallel to the Australian Margin (Stickley et al., 2004b), suggests that low potential for compounds to have been produced in areas with large differences in temperatures.

5.2 Site 1168 Sea Surface Temperature Trends

5.2.1 Sensitivity of temperature trends to latitudinal movement and setting

Aliasing of high frequency orbital variability in SST, as well as the latitudinal movement of the site, may affect the long-term temperature trends observed at this site. To reduce the influence of high frequency variability on long-term SST variation, we also present a smooth of the long-term trend by applying a local polynomial regression model (LOESS) (Figure 5). The smoothed trend shows a long term warming of 5°C from the Middle to the Late Oligocene, reaches a maximum around 26°C during the transition from the Oligocene to the Miocene, and then cools down to stablize at 24.5°C until the end of the record at 16.7 Ma.

Since the South Tasmanian margin has drifted northwards from paleolatitude of 55°S to 48°S over the Oligocene to Miocene interval sampled here, we follow the approach described by Herbert et al. (2016) to distinguish the component of SST change due to regional climate variation, from that due to the migration of the site to warmer latitudes. We calculate a temperature anomaly as the difference between the smoothed LOESS-fit temperatures for ODP Site 1168 (Figure 5) and the modern mean annual temperature (Locarnini et al., 2013) at the backtracked paleolatitude and longitude of Site 1168 position at the age of each $U_{37}^{k'}$ sample. Paleogeography is reconstructed according to (van Hinsbergen et al., 2015) which is based on the paleo magnetic reference frame of (Torsvik et al., 2012). The estimated anomaly reaffirms that there is a regional warming in the Late Oligocene by 4° which is not an artefact of the migration of the site. The calculated anomaly also indicates a relatively colder Early Miocene. Because the paleolatitude range of Site 1168 spans the modern Polar Front (PF) region of steepened temperature gradients, whereas the micropaleontological assemblages at multiple sites indicate that the PF remained poleward of Site 1168 in the Oligocene-Miocene (Scher et al., 2015), the corrected temperature anomaly may underestimate the actual regional warming through the Oligocene to Early Miocene.

We propose that the SST trends obtained from Site 1168 between 29.2 Ma and 16.7 Ma are representative of regional warming/cooling because they postdate the reorganization of ocean currents accompanying basin opening and the northward shift of the Tasmanian margin (Stickley et al., 2004b). Neodymium isotopes on fossil fish teeth at Site 1168 confirm the eastward flow from the Pacific Ocean in intermediate depths following the northward migration of the gateway into the influence of the westerly wind achieved by 29 Ma (Scher et al., 2015). Paleobathymetry reconstructions further support the existence of an important shallow to intermediate water exchange already by 30 Ma (Hochmuth et al., 2020).

5.2.2 Late Oligocene – Early Miocene SST trends

Our Southern Hemisphere SST record commences a few million years after the abrupt decrease in deep ocean temperature and increase in Antarctic ice volume recorded by benthic

$\delta^{18}O$ across the EOT (Figure 5). Our record begins within the MOGI, defined by oxygen isotope records and a 2-myr lowstand sea level (Liebrand et al., 2017; Miller et al., 2020), and we record relatively cool SST. The most prominent feature of our SST record is the warming of up to 5.5°C in the LOESS-smoothed record represented by 4°C increase in the calculated SST anomaly, from ca 29 to 24.5 Ma. This long term warming is simultaneous, within the age uncertainty, with the negative long term benthic $\delta^{18}O$ shift starting at 27 Ma (De Vleeschouwer et al., 2017; Zachos et al., 2001) described as the Late Oligocene Warming (Pekar et al., 2006; Villa and Persico, 2006).

The transient cooling and ice build-up reflected in a large positive benthic excursion at the Oligocene Miocene boundary was likely not sampled by the resolution of this study. Light reflectivity (L*) generated by the shipboard expedition (Exon et al., 2001), does present a significant turning point at the surrounding depths of the expected OMT applying the age model from Guitián et al. (2020) used in this study (Figure **S3**), coincident with turnover rates of sediment accumulation, where SST is not sampled. These data suggest that our smoothed trends over the Oligocene Miocene transition do omit some shorter duration transient events.

Our estimates of temperature anomaly suggest a colder Early Miocene than latest Oligocene, with a 1-myr. cooling of 2°C starting at 22.7 Ma, then stabilization of absolute temperatures around 24°C thereafter until 16.7 Ma (Figure 5). Those estimates are in agreement with relatively lower sea level reconstructions in the Early Miocene, and more positive benthic $\delta^{18}O$, although benthic records feature higher variability than Miocene SST at ODP 1168.

5.2.3 Amplitude of high frequency temperature variability at Site 1168

Although the low-resolution sampling of Site 1168 SST does not capture high frequency orbital scale variability, the observed short-term variations might reflect part of the orbital scale temperature amplitude. During Late Oligocene Warming, the higher frequency variability is of more than 5°C, at a time characterized by up to 1‰ 110kyr-modulated fluctuations in benthic $\delta^{18}O$ (De Vleeschouwer et al., 2017; Liebrand et al., 2016; Liebrand et al., 2017).

At the Antarctic margin Wilkes Land Site 1356, SST estimates also suggest highly dynamic surface temperatures in the surroundings of Antarctica. GDGT-derived temperature vary within the 6°C and are interpreted as glacial and interglacial intervals supported by pollen, dinoflagellates assemblages, and occasional carbonaceous facies (Bijl et al., 2018; Salabarnada et al., 2018; Sangiorgi et al., 2018). Further evidence of large amplitude cycles at the abyssal plain of the Wilkes Land exists from a recent revision of DSDP Site 269 sedimentation, suggesting a variability of 3°C to 5°C of GDGTs-derived SST during the 23 to 24 Ma time interval (Evangelinos et al., 2020) coeval with a oceanic front migration forced by interglacial and glacial cyclicity. Other low resolution Atlantic sites already suggested high amplitude of SST while $\delta^{18}O$ from same sample benthic foraminifera remained invariable (Guitián et al., 2019). Simultaneously, in the Antarctic continent mean annual temperature variability in the Oligocene to Miocene time interval suggest variation within 3°C (Passchier et al., 2013).

Reconstructions of SST at the bottom water formation areas currently derived from deep-water temperature records based on Mg/Ca from benthic foraminifera (Billups and Schrag, 2002; Cramer et al., 2011; Lear et al., 2004) show in orbital timescales temperatures within 3°C variability (Lear et al., 2004; Miller et al., 2020) (Figure 5). However, the evaluation of effects of fluctuations in carbonate ion or heterogeneity in seawater Mg/Ca (ie Lebrato et al., 2020) may lead to revisions of these temperatures.

The aggregate evidence for orbital variability in high latitude temperatures observed at Site 1168 and at other regional records near Antarctica, suggests that the assumption of dominant or exclusive ice volume regulation of benthic $\delta^{18}O$ (Liebrand et al., 2017) may require re-evaluation. If 3°C to 5°C orbital scale temperature changes observed at this high latitudes is transferred to bottom waters, it could lead to 1 ‰ variation in $\delta^{18}O$ of benthic foraminifera, potentially a significant portion of the observed benthic signal. Further high latitude SST reconstructions at high-resolution with additional benthic isotopes from same age frame would provide confirmation of the relative contribution of ice volume and temperature components.

5.3 Evolution of temperature gradients in the Southern Ocean

Attempts to capture global SST at the this time post-EOT and the entire Oligocene from alkenone-derived SST signal are limited by both the resolution as well as discontinuous records in the Southern Hemisphere. Our new estimates from Site 1168 provides new evidence of long-term SST trends over the Oligocene and Early Miocene. We examine here the temperature gradients between Site 1168 and other locations in the Southern Ocean.

In the Indo-Pacific sector of the Southern Ocean, the Early Oligocene average temperatures reconstructed at Site 1168 (28-29 Ma) are on average 2.3°C cooler than the GDGTs-derived temperatures at nearby Site 1172 at 30 Ma (Houben et al., 2019) (Figure 1; Table S1). As these sites had comparable paleolatitudes, the difference is potentially attributable to poleward surface ocean currents warming Site 1172. Compared to temperatures estimated at a 33 Ma time slice East of the Tasmanian Gateway at DSDP 277 (Liu et al., 2009), our oldest temperature estimates are only 3.1°C and 4.7°C colder than alkenone and GDGT-derived reconstructed temperatures, respectively .

In the Atlantic sector of the Southern Ocean at ODP Site 1090, with estimated paleolatitude 7° equatorward of Site 1168, average alkenone-derived temperatures are 3.1°C warmer than Site 1168 in the Early Oligocene (27.7 to 33 Ma)(Liu et al., 2009). This temperature difference is in agreement with the modelled latitudinal gradient for post EOT times (Kennedy-Asser et al., 2020). However, Early Oligocene temperature estimates at ODP Site 511, east of the Drake Passage in the South Atlantic, are cooler than ODP Site 1168 despite similar latitudes: averaging 9°C alkenone -derived and 15°C GDGTs-derived temperatures by 31-32.5 Ma (Houben et al., 2019; Liu et al., 2009). These low temperatures are thus inconsistent with the expected latitudinal gradients from modelling (Kennedy-Asser et al., 2020), suggesting that some oceanographic feature is driving temperature at this location.

On the Wilkes Land Antarctic margin, detailed GDGTs-derived SST reconstructions for Site 1356 (60°S, Figure 1 Map) span the interval from 33 Ma -22.7 Ma (Hartman et al., 2018; Salabarnada et al., 2018) (Figure 6). Paleogeography reconstructions suggest this site had a similar paleo- and modern latitude of 60°S (Torsvik et al., 2012; van Hinsbergen et al., 2015). During the MOGI, temperatures at Site 1356 are slightly cooler than those from Site 1168, as expected for the more poleward latitude of Site 1356 (Figure 6). However, while the strong Late Oligocene Warming is evident at Site 1168, no comparable warming is recorded on the Wilkes Land Antarctic Margin. Assuming the GDGTs-temperature at Wilkes land margin accurately records changes in surface temperature during this time period without bias from reworking or multiple sources (Bijl et al., 2018; Hartman et al., 2018), the increasing thermal gradient between Site 1168 and the Wilkes land margin might be explained by significant changes in ocean heat transport. One explanation for the Early Oligocene, is that Wilkes Land section of the Antarctic margin might be under the influence of the poleward extension of the proto-Leeuwin warm current (west-east in the south Australian margin), which would influence also the Western Tasmanian Margin where Site 1168 is located (Hartman et al., 2018; Stickley et al., 2004b). Potentially, the final opening of the Tasmanian Gateway increased east-west exchange by 27.5 Ma, diminished the significance of this warm poleward current and led instead to the alignment of the westerlies winds with the Drake passage and a gradual strengthening of the proto-Antarctic Circumpolar Current (ACC) (Exon et al., 2001; Nicholson and Stow, 2019; Pfuhl and McCave, 2005; Pfuhl et al., 2004; Scher et al., 2015). This would reduce the heat transport towards the Wilkes Land Antarctic margin. At this time interval the equivalent PF would be placed from 60°S to 64°S at the Late Oligocene to Early Miocene (Nelson and Cooke, 2001; Scher et al., 2015) and highly dynamic (Evangelinos et al., 2020) at least from 23 to 24 ma. Similar to the Wilkes Land Antarctic margin SST records, the benthic Mg/Ca bottom water temperature record also shows no significant Late Oligocene Warming (Figure 5) (Lear et al., 2004; Miller et al., 2020). Potentially, a similar mechanism of increasing polar isolation of the deep-water formation areas by the strengthening ACC is responsible.

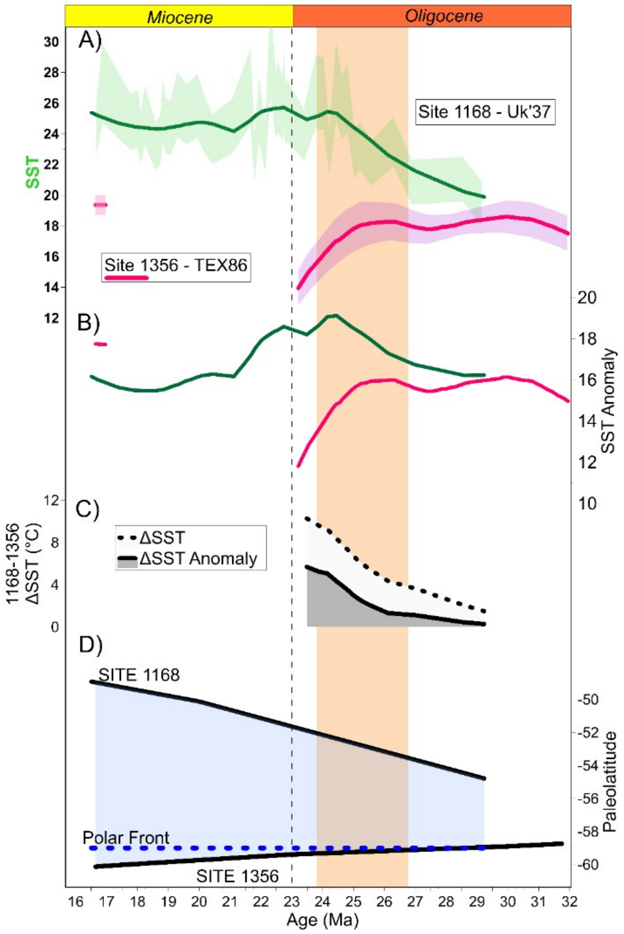

Figure 6. (**a**) SST reconstructions from $U^{k'}_{37}$ODP 1168 and TEX_{86} ODP 1356 (Hartman et al., 2018). (**b**) Reconstructed SST anomaly for both sites. (**c**) Temperature gradient between ODP 1168 and ODP 1356. (**d**) Paleolatitude estimations for both sites ODP 1356 (Torsvik et al., 2012; van Hinsbergen et al., 2015) and estimated position of the PF between the two sites (Salabarnada et al., 2018; Scher et al., 2015) using same paleolatitude reconstruction frame.

Data in the Southern Ocean are much more limited after the OMT. Across the OMT, terrestrial indicators suggest minimal vegetation change, with a landscape similar to the modern tundra in the continent (DSDP 270; also seen at CRP-2 Kulhanek et al. (2019)) and colder SST in the area with ice sheet grounding-line distal confirming the generally colder Early Miocene. By the mid Miocene (16.7 Ma) in Site 1168, 24°C water bathed the area. This estimation is consistent with recent TEX_{86} reconstructions at Site 1171, located only 700 km further south east (Figure 1), indicating mid Miocene temperatures of 26°C at 15.5 Ma (Leutert et al., 2020), 5.5°C warmer than TEX_{86} temperatures found at the Antarctic Margin (Hartman et al., 2018).

5.4 Late Oligocene Warming magnitude in the Southern and Northern Hemisphere

The magnitude of the Late Oligocene Warming observed in sea surface temperature records differs by latitude in both hemispheres for different proxy estimates (Figure 7).

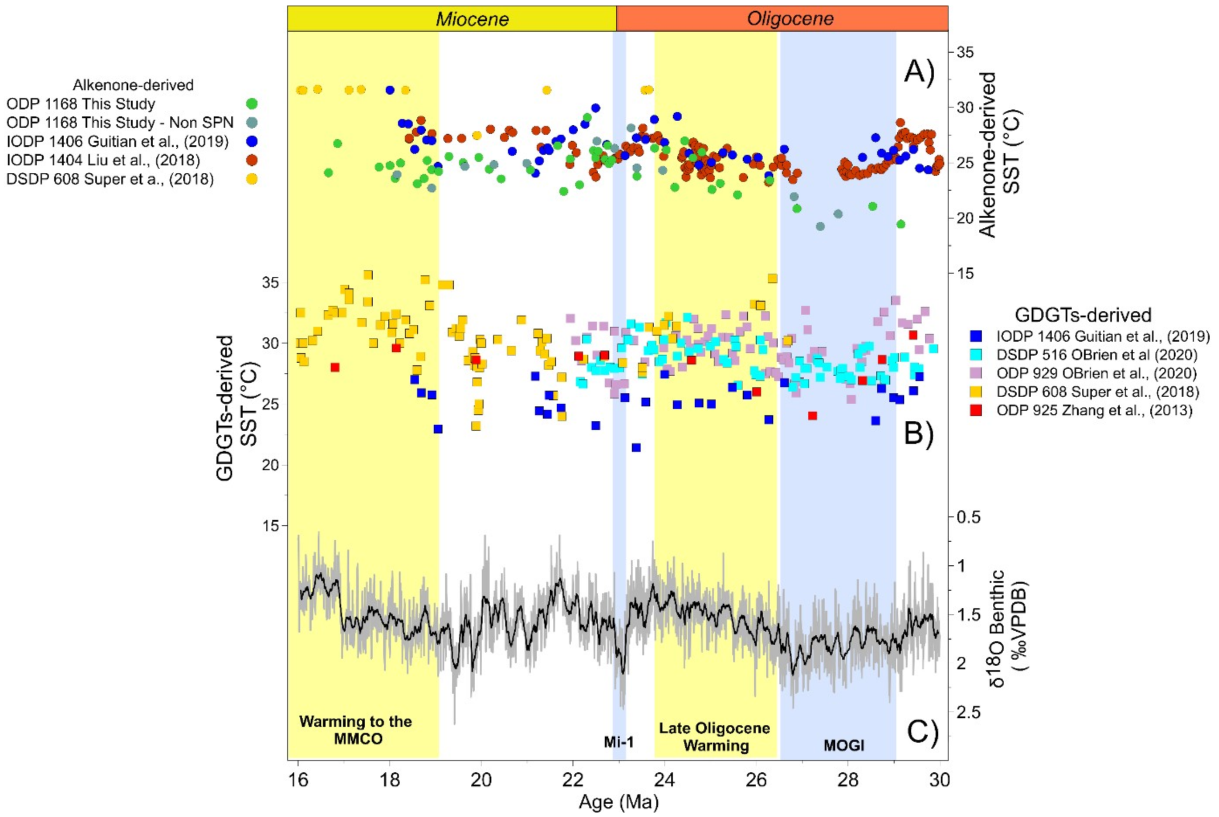

Figure 7. Oligocene to Miocene long-term SST records from low to mid latitude sites classified by proxy. (**a**) Alkenone-derived SST calibrated from the $U^{k'}_{37}$ratio with BAYSPLINE (Tierney and Tingley, 2018). (**b**) GDGTs-derived SST from TEX_{86} using BAYSPARE calibration (Tierney and Tingley, 2015). Note that SST records are presented without adjustment for latitudinal shift at any site as it is likely that only Site 1168 present significant anomaly. Both SST axis show equivalent magnitude. Vertical yellow and blue bands show main warming and cold period discussed in the text. (**c**) Benthic reference megasplice (De Vleeschouwer et al., 2017).

Alkenone-derived temperatures from 40°N Atlantic Site 1406, and referenced to benthic- $\delta^{18}O$ records at that site, show a ca 3°C warmer Late Oligocene than the preceeding Early Oligocene (Guitián et al., 2019). However, a 2-myr hiatus interrupts the record from 28 to 26 Ma. Higher resolution alkenone-SST record at nearby IODP Site 1404 describes a 1-myr cooling up to 3°C after the EOT ending at 27.9 Ma (Liu et al., 2018). After a 1-myr unsampled interval, SST increases by 4°C from 26.8 to 23.5 Ma. Despite the temporal gaps, those alkenone-SST records appear to be in agreement with the magnitude obtained in Site 1168: the Late Oligocene warming of 5.5°C from 29 Ma to the stabilization at 24.5 Ma, is equivalent to 4°C of SST-anomaly after adjustment for latitudinal movement of the site.

A comparison with GDGTs-derived temperature reconstructions shows distinct magnitude. Additionally, those reconstructions show more scattered estimations than equivalent resolution studies from the alkenone proxy (i. e. Site 1404). Recent 100ky-resolution reconstructions at Equatorial Atlantic ODP Site 929 show no evident warming over the entire Late Oligocene -Miocene, and if there is one, appear to be only 2.5°C from 26.5 Ma to 25.5

Ma (O'Brien et al., 2020). Some previous low resolution attempts to reconstruct low latitude SST have shown a significant 5°C warming from 27 Ma to 25.3 Ma at Site 925 according to GDGTs (Zhang et al., 2013), however, coeval $U^{k'}_{37}$ show clear saturation of tri-unsaturated C_{37} alkenone, meaning temperature must be over 31°C using most updated calibrations. At mid-latitude Sites DSDP 608 and IODP Site 1406, GDGT-derived SST does not support either any warming in the Oligocene (Guitián et al., 2019; Super et al., 2018); where resolution is considerable during the Miocene, the Oligocene time interval is barely sampled.

At the same time, southern mid-latitude Atlantic Site 516 GDGTs-reconstructions identify a clear increase of the mean temperature but however, show only a 1.5°C increase from 27.5 to 24 Ma with no colder temperature sampled older in the middle Oligocene (O'Brien et al., 2020).

This comparison clearly suggests that further interpretations need to be done using both proxies and that higher resolution alkenone-derived studies are required to interpret if warmings are equivalent between latitudes and if there is significant polar amplification of the multi-million year scale temperature changes.

6. Conclusions

The Tasmanian Sea ODP Site 1168 alkenone-derived SST record shows for the first time cold conditions related with the MOGI, and confirms in the Southern Hemisphere the previously recognized subsequent long term warming of the Late Oligocene Warming. By 29 Ma, 20°C characterized the middle Oligocene at Site 1168, followed by 5°C increase of average reconstructed temperatures to 24.5 Ma linked to the end the MOGI. Apparent warmer temperatures exist during the latest Oligocene and transition to the Miocene around 24.5-22.5°C, cooling down 2°C to finally stabilize into the Miocene around 20.1 Ma, although the Oligocene Miocene boundary might not be sampled here. The variability of SST is higher in the warm Late Oligocene and more stable in the relatively colder Early Miocene. Reconstructed latitudinal drift of the site does not explain the observed long term temperature trends; rather these trends represent true temperature anomalies for a given latitude. Comparison with previously published records from the Atlantic Ocean and surrounding Antarctic locations, highlights the discrepancy in warming amplitude among proxies and locations and emphasizes the importance of first, paleoceanographic circulations patterns and second, the understanding of the different proxies sources, to interpret southern hemisphere temperature gradients.

7. Acknowledgments and Data

Sediment samples were provided by the Ocean Drilling Program (ODP). This study was supported by the Swiss National Science Foundation (Award 200021_182070 to Heather Stoll). Authors are very thankful to Madalina Jaggi, Stewart Bishop, and Thierry Solms for assistance in the laboratory. We also thank Lena Thöle and Mariska Hoorweg for providing the subset of samples from Utrecht University with an ERC starting grant n802835 OceaNice to Peter K. Bijl. Data generated for this work is uploaded as independent excel file as Supplementary Information Table S2 and archived online at Zenodo Data Archive (link will be provided once manuscript is accepted).

8. References

Bijl, P.K., Houben, A.J., Hartman, J.D., Pross, J., Salabarnada, A., Escutia, C., Sangiorgi, F., 2018. Paleoceanography and ice sheet variability offshore Wilkes Land, Antarctica-Part 2: Insights from Oligocene-Miocene dinoflagellate cyst assemblages. Climate of the Past 14, 1015-1033.

Billups, K., Schrag, D., 2002. Paleotemperatures and ice volume of the past 27 Myr revisited with paired Mg/Ca and 18O/16O measurements on benthic foraminifera. Paleoceanography 17, 3-1-3-11.

Brassell, S., Eglinton, G., Marlowe, I., Pflaumann, U., Sarnthein, M., 1986. Molecular stratigraphy: a new tool for climatic assessment. Nature 320, 129.

Brassell, S.C., 1993. Applications of biomarkers for delineating marine paleoclimatic fluctuations during the Pleistocene, Organic Geochemistry. Springer, pp. 699-738.

Conte, M.H., Eglinton, G., 1993. Alkenone and alkenoate distributions within the euphotic zone of the eastern North Atlantic: correlation with production temperature. Deep Sea Research Part I: Oceanographic Research Papers 40, 1935-1961.

Conte, M.H., Thompson, A., Lesley, D., Harris, R.P., 1998. Genetic and physiological influences on the alkenone/alkenoate versus growth temperature relationship in Emiliania huxleyi and Gephyrocapsa oceanica. Geochimica et Cosmochimica Acta 62, 51-68.

Cramer, B., Miller, K., Barrett, P., Wright, J., 2011. Late Cretaceous–Neogene trends in deep ocean temperature and continental ice volume: Reconciling records of benthic foraminiferal geochemistry (δ18O and Mg/Ca) with sea level history. Journal of Geophysical Research: Oceans 116.

D'Andrea, W.J., Theroux, S., Bradley, R.S., Huang, X., 2016. Does phylogeny control U37K-temperature sensitivity? Implications for lacustrine alkenone paleothermometry. Geochimica et Cosmochimica Acta 175, 168-180.

De Vleeschouwer, D., Vahlenkamp, M., Crucifix, M., Pälike, H., 2017. Alternating Southern and Northern Hemisphere climate response to astronomical forcing during the past 35 my. Geology 45, 375-378.

Evangelinos, D., Escutia, C., Etourneau, J., Hoem, F., Bijl, P., Boterblom, W., van de Flierdt, T., Valero, L., Flores, J.-A., Rodriguez-Tovar, F.J., 2020. Late oligocene-miocene proto-antarctic circumpolar current dynamics off the Wilkes Land margin, East Antarctica. Global and Planetary Change, 103221.

Exon, N., Kennett, J., Malone, M., 2001. 1. LEG 189 SUMMARY, Proceedings of the Ocean Drilling Program.

Exon, N., Kennett, J., Malone, M., Brinkhuis, H., Chaproniere, G., Ennyu, A., Fothergill, P., Fuller, M., Grauert, M., Hill, P., 2002. Drilling reveals climatic consequences of Tasmanian Gateway opening. Eos, Transactions American Geophysical Union 83, 253-259.

Gong, C., Hollander, D.J., 1999. Evidence for differential degradation of alkenones under contrasting bottom water oxygen conditions: Implication for paleotemperature reconstruction. Geochimica et Cosmochimica Acta 63, 405-411.

Gradstein, F.M., Ogg, J.G., Schmitz, M., Ogg, G., 2012. The geologic time scale 2012. elsevier.

Grimalt, J.O., Rullkötter, J., Sicre, M.A., Summons, R., Farrington, J., Harvey, H.R., Goñi, M., Sawada, K., 2000. Modifications of the C37 alkenone and alkenoate composition in the water column and sediment: Possible implications for sea surface temperature estimates in paleoceanography. Geochemistry, Geophysics, Geosystems 1.

Guitián, J., Dunkley Jones, T., Hernández-Almeida, I., Löffel, T., Stoll, H.M., 2020. Adaptations of coccolithophore size to selective pressures during the Oligocene - Early Miocene high CO2 world. Paleoceanography and Paleoclimatology n/a, e2020PA003918.

Guitián, J., Phelps, S., Polissar, P.J., Ausín, B., Eglinton, T.I., Stoll, H.M., 2019. Midlatitude Temperature Variations in the Oligocene to Early Miocene. Paleoceanography and Paleoclimatology 34, 1328-1343.

Hartman, J.D., Sangiorgi, F., Escutia Dotti, C., 2018. Paleoceanography and ice sheet variability offshore Wilkes Land, Antarctica–Part 3: Insights from Oligocene–Miocene TEX86-based sea surface temperature reconstructions.

Herbert, T.D., Lawrence, K.T., Tzanova, A., Peterson, L.C., Caballero-Gill, R., Kelly, C.S., 2016. Late Miocene global cooling and the rise of modern ecosystems. Nature Geoscience 9, 843.

Hill, P.J., Exon, N.F., 2004. Tectonics and basin development of the offshore Tasmanian area incorporating results from deep ocean drilling. GMS 151, 19-42.

Hochmuth, K., Gohl, K., Leitchenkov, G., Sauermilch, I., Whittaker, J.M., Uenzelmann−Neben, G., Davy, B., De Santis, L., 2020. The evolving paleobathymetry of the circum−Antarctic Southern Ocean since 34 Ma: A key to understanding past cryosphere−ocean developments. Geochemistry, Geophysics, Geosystems 21, e2020GC009122.

Houben, A.J., Bijl, P.K., Sluijs, A., Schouten, S., Brinkhuis, H., 2019. Late Eocene Southern Ocean cooling and invigoration of circulation preconditioned Antarctica for full−scale glaciation. Geochemistry, Geophysics, Geosystems 20, 2214-2234.

Kaiser, J., van der Meer, M.T., Arz, H.W., 2017. Long-chain alkenones in Baltic Sea surface sediments: new insights. Organic Geochemistry 112, 93-104.

Kennedy-Asser, A.T., Lunt, D.J., Valdes, P.J., Ladant, J.-B., Frieling, J., Lauretano, V., 2020. Changes in the high-latitude Southern Hemisphere through the Eocene–Oligocene transition: a model–data comparison. Climate of the Past 16.

Kulhanek, D.K., Levy, R.H., Clowes, C.D., Prebble, J.G., Rodelli, D., Jovane, L., Morgans, H.E., Kraus, C., Zwingmann, H., Griffith, E.M., 2019. Revised chronostratigraphy of DSDP Site 270 and late Oligocene to early Miocene paleoecology of the Ross Sea sector of Antarctica. Global and Planetary Change 178, 46-64.

Lear, C.H., Rosenthal, Y., Coxall, H.K., Wilson, P., 2004. Late Eocene to early Miocene ice sheet dynamics and the global carbon cycle. Paleoceanography 19.

Lebrato, M., Garbe-Schönberg, D., Müller, M.N., Blanco-Ameijeiras, S., Feely, R.A., Lorenzoni, L., Molinero, J.-C., Bremer, K., Jones, D.O., Iglesias-Rodriguez, D., 2020. Global variability in seawater Mg: Ca and Sr: Ca ratios in the modern ocean. Proceedings of the National Academy of Sciences 117, 22281-22292.

Leutert, T.J., Auderset, A., Martínez-García, A., Modestou, S., Meckler, A.N., 2020. Coupled Southern Ocean cooling and Antarctic ice sheet expansion during the middle Miocene. Nature Geoscience 13, 634-639.

Liebrand, D., Beddow, H.M., Lourens, L.J., Pälike, H., Raffi, I., Bohaty, S.M., Hilgen, F.J., Saes, M.J., Wilson, P.A., van Dijk, A.E., 2016. Cyclostratigraphy and eccentricity tuning of the early Oligocene through early Miocene (30.1–17.1 Ma): Cibicides mundulus stable oxygen and carbon isotope records from Walvis Ridge Site 1264. Earth and Planetary Science Letters 450, 392-405.

Liebrand, D., de Bakker, A.T., Beddow, H.M., Wilson, P.A., Bohaty, S.M., Ruessink, G., Palike, H., Batenburg, S.J., Hilgen, F.J., Hodell, D.A., Huck, C.E., Kroon, D., Raffi, I., Saes, M.J., van Dijk, A.E., Lourens, L.J., 2017. Evolution of the early Antarctic ice ages. Proc Natl Acad Sci U S A 114, 3867-3872.

Liu, Z., He, Y., Jiang, Y., Wang, H., Liu, W., Bohaty, S.M., Wilson, P.A., 2018. Transient temperature asymmetry between hemispheres in the Palaeogene Atlantic Ocean. Nature Geoscience 11, 656.

Liu, Z., Pagani, M., Zinniker, D., Deconto, R., Huber, M., Brinkhuis, H., Shah, S.R., Leckie, R.M., Pearson, A., 2009. Global cooling during the eocene-oligocene climate transition. Science 323, 1187-1190.

Locarnini, R., Mishonov, A., Antonov, J., Boyer, T., Garcia, H., Baranova, O., Zweng, M., Paver, C., Reagan, J., Johnson, D., 2013. World Ocean Atlas 2013, Volume 1: Temperature, edited by: Levitus, S. A. Mishonov Technical Ed., NOAA Atlas NESDIS 73, 40.

Longo, W.M., Dillon, J.T., Tarozo, R., Salacup, J.M., Huang, Y., 2013. Unprecedented separation of long chain alkenones from gas chromatography with a poly (trifluoropropylmethylsiloxane) stationary phase. Organic Geochemistry 65, 94-102.

Longo, W.M., Theroux, S., Giblin, A.E., Zheng, Y., Dillon, J.T., Huang, Y., 2016. Temperature calibration and phylogenetically distinct distributions for freshwater alkenones: Evidence from northern Alaskan lakes. Geochimica et Cosmochimica Acta 180, 177-196.

Lopez, J.F., de Oteyza, T.G., Teixidor, P., Grimalt, J.O., 2005. Long chain alkenones in hypersaline and marine coastal microbial mats. Organic Geochemistry 36, 861-872.

Marlowe, I., Brassell, S., Eglinton, G., Green, J., 1990. Long-chain alkenones and alkyl alkenoates and the fossil coccolith record of marine sediments. Chemical Geology 88, 349-375.

Mcgonigal, K.L., 2004. Quantitative Miocene calcareous nannofossil biostratigraphy from the Tasmanian Gateway. GMS 151, 191-213.

Miller, K.G., Browning, J.V., Schmelz, W.J., Kopp, R.E., Mountain, G.S., Wright, J.D., 2020. Cenozoic sea-level and cryospheric evolution from deep-sea geochemical and continental margin records. Science advances 6, eaaz1346.

Nelson, C.S., Cooke, P.J., 2001. History of oceanic front development in the New Zealand sector of the Southern Ocean during the Cenozoic—a synthesis. New Zealand Journal of geology and geophysics 44, 535-553.

Nicholson, U., Stow, D., 2019. Erosion and deposition beneath the Subantarctic Front since the Early Oligocene. Scientific reports 9, 1-9.

O'Neill, C., Müller, D., Steinberger, B., 2005. On the uncertainties in hot spot reconstructions and the significance of moving hot spot reference frames. Geochemistry, Geophysics, Geosystems 6.

O'Brien, C.L., Huber, M., Thomas, E., Pagani, M., Super, J.R., Elder, L.E., Hull, P.M., 2020. The enigma of Oligocene climate and global surface temperature evolution. Proceedings of the National Academy of Sciences 117, 25302-25309.

Passchier, S., Bohaty, S.M., Jiménez−Espejo, F., Pross, J., Röhl, U., van de Flierdt, T., Escutia, C., Brinkhuis, H., 2013. Early Eocene to middle Miocene cooling and aridification of East Antarctica. Geochemistry, Geophysics, Geosystems 14, 1399-1410.

Pekar, S.F., DeConto, R.M., 2006. High-resolution ice-volume estimates for the early Miocene: Evidence for a dynamic ice sheet in Antarctica. Palaeogeography, Palaeoclimatology, Palaeoecology 231, 101-109.

Pekar, S.F., DeConto, R.M., Harwood, D.M., 2006. Resolving a late Oligocene conundrum: deep-sea warming and Antarctic glaciation. Palaeogeography, Palaeoclimatology, Palaeoecology 231, 29-40.

Pfuhl, H.A., McCave, I.N., 2003. Integrated age models for the early Oligocene-early Miocene, sites 1168 and 1170–1172, Proc. ODP, Sci. Results, pp. 1-21.

Pfuhl, H.A., McCave, I.N., 2005. Evidence for late Oligocene establishment of the Antarctic Circumpolar Current. Earth and Planetary Science Letters 235, 715-728.

Pfuhl, H.A., Mccave, I.N., Schellenberg, S.A., Ferretti, P., 2004. Changes in Southern Ocean circulation in late Oligocene to early Miocene time, The Cenozoic Southern Ocean: Tectonics, Sedimentation, and Climate Change Between Australia and Antarctica. American Geophysical Union Washington/DC, pp. 173-189.

Prahl, F.G., Mix, A.C., Sparrow, M.A., 2006. Alkenone paleothermometry: Biological lessons from marine sediment records off western South America. Geochimica et Cosmochimica Acta 70, 101-117.

Prahl, F.G., Wakeham, S.G., 1987. Calibration of unsaturation patterns in long-chain ketone compositions for palaeotemperature assessment. Nature 330, 367.

Rechka, J., Maxwell, J., 1988. Unusual long chain ketones of algal origin. Tetrahedron Letters 29, 2599-2600.

Rosell-Melé, A., Carter, J., Eglinton, G., 1994. Distributions of long-chain alkenones and alkyl alkenoates in marine surface sediments from the North East Atlantic. Organic Geochemistry 22, 501-509.

Salabarnada, A., Escutia, C., Röhl, U., Nelson, C.H., McKay, R., Jiménez-Espejo, F., Bijl, P., Hartman, J., Strother, S., Salzmann, U., 2018. Paleoceanography and ice sheet variability offshore Wilkes Land, Antarctica–Part 1: Insights from late Oligocene astronomically paced contourite sedimentation. Climate of the Past 14, 991-1014.

Sangiorgi, F., Bijl, P.K., Passchier, S., Salzmann, U., Schouten, S., McKay, R., Cody, R.D., Pross, J., Van De Flierdt, T., Bohaty, S.M., 2018. Southern Ocean warming and Wilkes Land ice sheet retreat during the mid-Miocene. Nature Communications 9, 1-11.

Scher, H.D., Whittaker, J.M., Williams, S.E., Latimer, J.C., Kordesch, W.E., Delaney, M.L., 2015. Onset of Antarctic Circumpolar Current 30 million years ago as Tasmanian Gateway aligned with westerlies. Nature 523, 580-583.

Stickley, C., Brinkhuis, H., McGonigal, K., Chaproniere, G., Fuller, M., Kelly, D., Nürnberg, D., Pfuhl, H., Schellenberg, S., Schönfeld, J., 2004a. Late Cretaceous–Quaternary biomagnetostratigraphy of ODP Sites 1168, 1170, 1171, and 1172, Tasmanian Gateway, Proceedings of the Ocean Drilling Program, Scientific Results. Ocean Drilling Program, College Station TX, pp. 1-57.

Stickley, C.E., Brinkhuis, H., Schellenberg, S.A., Sluijs, A., Röhl, U., Fuller, M., Grauert, M., Huber, M., Warnaar, J., Williams, G.L., 2004b. Timing and nature of the deepening of the Tasmanian Gateway. Paleoceanography 19.

Super, J.R., Thomas, E., Pagani, M., Huber, M., O'Brien, C., Hull, P.M., 2018. North Atlantic temperature and p CO2 coupling in the early-middle Miocene. Geology 46, 519-522.

Theroux, S., D'Andrea, W.J., Toney, J., Amaral-Zettler, L., Huang, Y., 2010. Phylogenetic diversity and evolutionary relatedness of alkenone-producing haptophyte algae in lakes: implications for continental paleotemperature reconstructions. Earth and Planetary Science Letters 300, 311-320.

Tierney, J.E., Tingley, M.P., 2015. A TEX(8)(6) surface sediment database and extended Bayesian calibration. Sci Data 2, 150029.

Tierney, J.E., Tingley, M.P., 2018. BAYSPLINE: A new calibration for the alkenone paleothermometer. Paleoceanography and Paleoclimatology 33, 281-301.

Torsvik, T.H., Steinberger, B., Cocks, L.R.M., Burke, K., 2008. Longitude: linking Earth's ancient surface to its deep interior. Earth and Planetary Science Letters 276, 273-282.

Torsvik, T.H., Van der Voo, R., Preeden, U., Mac Niocaill, C., Steinberger, B., Doubrovine, P.V., Van Hinsbergen, D.J., Domeier, M., Gaina, C., Tohver, E., 2012. Phanerozoic polar wander, palaeogeography and dynamics. Earth-Science Reviews 114, 325-368.

van Hinsbergen, D.J., de Groot, L.V., van Schaik, S.J., Spakman, W., Bijl, P.K., Sluijs, A., Langereis, C.G., Brinkhuis, H., 2015. A paleolatitude calculator for paleoclimate studies. PloS one 10.

Villa, G., Persico, D., 2006. Late Oligocene climatic changes: evidence from calcareous nannofossils at Kerguelen Plateau Site 748 (Southern Ocean). Palaeogeography, Palaeoclimatology, Palaeoecology 231, 110-119.

Volkman, J.K., Eglinton, G., CoRNER, E.D., Forsberg, T., 1980. Long-chain alkenes and alkenones in the marine coccolithophorid Emiliania huxleyi. Phytochemistry 19, 2619-2622.

Wei, W., McGonigal, K.L., Zhong, S., 2003. Data report: Paleogene calcareous nannofossil biostratigraphy of ODP Leg 189 (Australia-Antarctica gateway), Proc. ODP, Sci. Results. Ocean Drilling Program College Station, TX, p. 114.

Westerhold, T., Marwan, N., Drury, A.J., Liebrand, D., Agnini, C., Anagnostou, E., Barnet, J.S., Bohaty, S.M., De Vleeschouwer, D., Florindo, F., 2020. An astronomically dated record of Earth's climate and its predictability over the last 66 million years. Science 369, 1383-1387.

Young, J.R., 1998. Neogene nannofossils. Calcareous Nannofossil Biostratigraphy. Kluwer Academic, Dordrecht 225, 265.

Zachos, J., Pagani, M., Sloan, L., Thomas, E., Billups, K., 2001. Trends, rhythms, and aberrations in global climate 65 Ma to present. Science 292, 686-693.

Zhang, Y.G., Pagani, M., Liu, Z., Bohaty, S.M., Deconto, R., 2013. A 40-million-year history of atmospheric CO(2). Philos Trans A Math Phys Eng Sci 371, 20130096.

Zheng, Y., Heng, P., Conte, M.H., Vachula, R.S., Huang, Y., 2019. Systematic chemotaxonomic profiling and novel paleotemperature indices based on alkenones and alkenoates: Potential for disentangling mixed species input. Organic Geochemistry 128, 26-41.

Zheng, Y., Tarozo, R., Huang, Y., 2017. Optimizing chromatographic resolution for simultaneous quantification of long chain alkenones, alkenoates and their double bond positional isomers. Organic Geochemistry 111, 136-143.